A unique squalenoylated and nonpegylated doxorubicin nanomedicine with systemic long-circulating properties and anticancer activity

Andrei Maksimenko[a], Franco Dosio[b], Julie Mougin[a], Annalisa Ferrero[b], Severine Wack[a], L. Harivardhan Reddy[a], Andrée-Anne Weyn[c], Elise Lepeltier[a], Claudie Bourgaux[a], Barbara Stella[b], Luigi Cattel[b], and Patrick Couvreur[a,1]

[a]Faculté de Pharmacie, Institut Galien Paris Sud, Université Paris Sud, Unité Mixte de Recherche, Centre National de la Recherche Scientifique 8612, 92296 Châtenay-Malabry Cedex, France; [b]Dipartimento di Scienza e Tecnologia del Farmaco, Università degli Studi di Torino, 10125 Turin, Italy; and [c]Department of Pharmacology, Centre de Recherches Biologiques, 18800 Baugy, France

Edited by Robert Langer, Massachusetts Institute of Technology, Cambridge, MA, and approved November 13, 2013 (received for review August 1, 2013)

We identified that the chemical linkage of the anticancer drug doxorubicin onto squalene, a natural lipid precursor of the cholesterol's biosynthesis, led to the formation of squalenoyl doxorubicin (SQ-Dox) nanoassemblies of 130-nm mean diameter, with an original "loop-train" structure. This unique nanomedicine demonstrates: (*i*) high drug payload, (*ii*) decreased toxicity of the coupled anticancer compound, (*iii*) improved therapeutic response, (*iv*) use of biocompatible transporter material, and (*v*) ease of preparation, all criteria that are not combined in the currently available nanodrugs. Cell culture viability tests and apoptosis assays showed that SQ-Dox nanoassemblies displayed comparable antiproliferative and cytotoxic effects than the native doxorubicin because of the high activity of apoptotic mediators, such as caspase-3 and poly(ADP-ribose) polymerase. In vivo experiments have shown that the SQ-Dox nanomedicine dramatically improved the anticancer efficacy, compared with free doxorubicin. Particularly, the M109 lung tumors that did not respond to doxorubicin treatment were found inhibited by 90% when treated with SQ-Dox nanoassemblies. SQ-Dox nanoassembly-treated MiaPaCa-2 pancreatic tumor xenografts in mice decreased by 95% compared with the tumors in the saline-treated mice, which was significantly higher than the 29% reduction achieved by native doxorubicin. Concerning toxicity, SQ-Dox nanoassemblies showed a fivefold higher maximum-tolerated dose than the free drug, and moreover, the cardiotoxicity study has evidenced that SQ-Dox nanoassemblies did not cause any myocardial lesions, such as those induced by the free doxorubicin treatment. Taken together, these findings demonstrate that SQ-Dox nanoassemblies make tumor cells more sensitive to doxorubicin and reduce the cardiac toxicity, thus providing a remarkable improvement in the drug's therapeutic index.

squalene-doxorubicin bioconjugate | pancreatic cancer | lung cancer

The design of nanodevices for the delivery of anticancer drugs to tumors has gained considerable interest for improving the treatment of neoplastic diseases (1–5), which offers a fresh interesting therapeutic approach because the discovery of novel anticancer agents with sufficient anticancer activity and acceptable tolerance is becoming more and more difficult. Ideally, anticancer nanomedicines should: (*i*) have high drug payload to avoid the need to administer excessively high amounts of carrier material; (*ii*) use safe and nontoxic carrier material, preferably of natural origin; (*iii*) improve the therapeutic response of the anticancer agent; (*iv*) allow a decrease of the undesired toxicity of the antitumor drug; and (*v*) be easy to prepare, ideally using a surfactant-free process. More often, the inability of nanomedicines in meeting the above criteria hinders their translation to clinics, as illustrated by the limited number of anticancer nanomedicines that have reached the market to date.

In this context, we have developed the "squalenoylation" technology, consisting of the chemical linkage of squalene, a natural and well-tolerated triterpene, with anticancer and antiviral nucleoside analogs (6). Those bioconjugates were observed to spontaneously self-assemble, in a surfactant-free aqueous medium, as nanoparticles having mean diameter of approximately 150 nm. Now, continuing on this trail, we have designed a squalenoyl derivative of doxorubicin that overtakes the previous results beyond all expectations in terms of anticancer activity improvement and toxicity reduction. Doxorubicin is one of the leading anticancer drugs in clinical oncology with a broad spectrum of activity against various solid and hematologic neoplastic diseases, and it is commonly present in several anticancer therapeutic regimens [funding sources: American Cancer Society (2011) Doxorubicin (7); Pfizer Inc. (2011) Doxorubicin Hydrochloride for Injection (8); National Cancer Institute (2011) Cancer Drug Information: Doxorubicin Hydrochloride (9)]. The effectiveness of doxorubicin is impeded by acute and subacute side effects, mainly dose-limiting irreversible cardiotoxicity and myelosuppression (10). In an attempt to reduce the side-effects of doxorubicin and to improve its anticancer efficacy, various nanocarriers of doxorubicin and daunorubicin have been developed, including micelles, dendrimers, solid-lipid, and polymer nanoparticles (11–15). Liposomes are by far the most studied nanoformulation of doxorubicin, and are the only products that reached the market (Caelyx, Myocet). In general, doxorubicin-loaded liposomes exhibit efficiencies comparable to those of the conventional anthracycline cytostatic agents but with less cardiotoxicity (16). The liposome formulation (Caelyx)

Significance

We identified that the chemical linkage of the anticancer drug doxorubicin onto squalene, a natural lipid precursor of the cholesterol's biosynthesis, led to the formation of squalenoyl doxorubicin nanoassemblies of 130-nm mean diameter, with an original "loop-train" structure. This unique nanomedicine demonstrates: (*i*) high drug payload, (*ii*) decreased toxicity of the coupled anticancer compound, (*iii*) improved therapeutic response, (*iv*) use of biocompatible transporter material, and (*v*) ease of preparation, all criteria that are not combined in the currently available nanodrugs. Taken together, these findings demonstrate that the squalenoylated doxorubicin nanoassemblies make tumor cells more sensitive to doxorubicin and reduce the cardiac toxicity.

Author contributions: A.M., F.D., and P.C. designed research; A.M., F.D., J.M., A.F., S.W., L.H.R., A.-A.W., E.L., C.B., B.S., and L.C. performed research; A.M., F.D., L.C., and P.C. contributed new reagents/analytic tools; A.M., F.D., and P.C. analyzed data; and A.M. and P.C. wrote the paper.

The authors declare no conflict of interest.

This article is a PNAS Direct Submission.

Freely available online through the PNAS open access option.

[1]To whom correspondence should be addressed. E-mail: patrick.couvreur@u-psud.fr.

This article contains supporting information online at www.pnas.org/lookup/suppl/doi:10.1073/pnas.1313459110/-/DCSupplemental.

surface-coated with hydrophilic polymer poly(ethylene glycol) (PEG) resulted in an increased systemic half-life as a result of reduced capture by the mononuclear phagocyte system (i.e., liver and spleen macrophages) (17). In experimental animal models, these long-circulating PEGylated liposomes were found to extravasate through the defects of the tumor vasculature by the so called "enhanced permeability and retention effect," thus allowing passive targeting to the neoplastic tissue (18). However, in clinical practice the administration of PEGylated liposomes loaded with doxorubicin was associated with palmar-plantar erythrodysesthesia ("hand-foot" syndrome), which may evolve into ulceration and epidermal necrosis if the chemotherapy cycle is not delayed (19). Hand-foot syndrome represents a major limitation in the Caelyx treatment, because it can adversely affect the quality of life of the patients, which may be addressed by dose-reduction strategy (20). In addition, recent studies have demonstrated that PEGylated liposomes can generate complement activation through increased alternative pathway turnover (21), which now provides a plausible explanation to the previously reported anaphylaxis, or is referred to as cardiovascular collapse in species that have received medicines containing poly (ethylene glycol) as a carrier/solubilizer (22). Finally, intravenous administration of PEGylated liposomes was shown to dramatically alter the pharmacokinetic behavior of the subsequently injected PEGylated liposomes, which may have important implications when repeated administrations are needed in many chemotherapeutic schedules (23, 24). Thus, there is a consensus in the drug-delivery community that new concepts are needed for the construction of long-circulating nanocarriers avoiding the use of PEG. Another concern is the low drug-loading (i.e., milligrams of the anticancer anthracycline per milligrams of carrier material), though the use of tansmembrane pH gradient-loading methods into liposomes varies from 0.05 μM/1 μM lipid to 0.21 μM/1 μM lipid (25, 26). With polymer nanoparticles, the maximum payload is generally less than 10% (wt/wt) (27). Because the effective dose in cancer therapy is dependent not only on nanoparticle/liposome localization at the tumor site but also on the maximum payload that each particle can deliver, drug-loading is certainly another key issue for efficient anticancer treatment. Additionally, in the cases where the drug encapsulation is performed by noncovalent technique, a risk of premature drug release may occur (the so-called "burst release") (28).

In this context, the present study proposes a unique doxorubicin nanomedicine with systemic long-circulating properties, without the use of PEG. The nanomedicine is based on the conjugation of doxorubicin to the 1,1′,2-Tris-norsqualenoic acid. Through careful design and synthesis, we have selected the C-14 ester derivative (squalenoyl doxorubicin, SQ-Dox), which by an easy solvent-displacement procedure led to the construction of nanoassemblies. Unexpectedly, we have observed that this conjugate was able to self-organize in water into unique "loop-train" elongated nanostructures with an impressive drug payload (i.e., 57%) and high stability. This nanomedicine has been shown to decrease importantly the overall toxicity, including the cardiac toxicity of doxorubicin and, additionally, considerable anticancer efficacy has been proven on both murine pulmonary and human pancreatic experimental cancers.

Results

Synthesis, Morphological Characterization, and Physicochemical Properties of SQ-Dox Nanoassemblies. The synthetic route to C-14 ester derivative (SQ-Dox) (Fig. 1*A*) entails the nucleophilic displacement-type esterification of 14-bromodaunorubicin hydrochloride (prepared by bromination of daunorubicin hydrochloride) with the salt of the 1,1′,2-Tris-norsqualenoic acid as indicated in *SI Materials and Methods* (Fig. S1). Addition of an organic phase, containing SQ-Dox dissolved in tetrahydrofuran (THF), into distilled water led to the spontaneous formation of

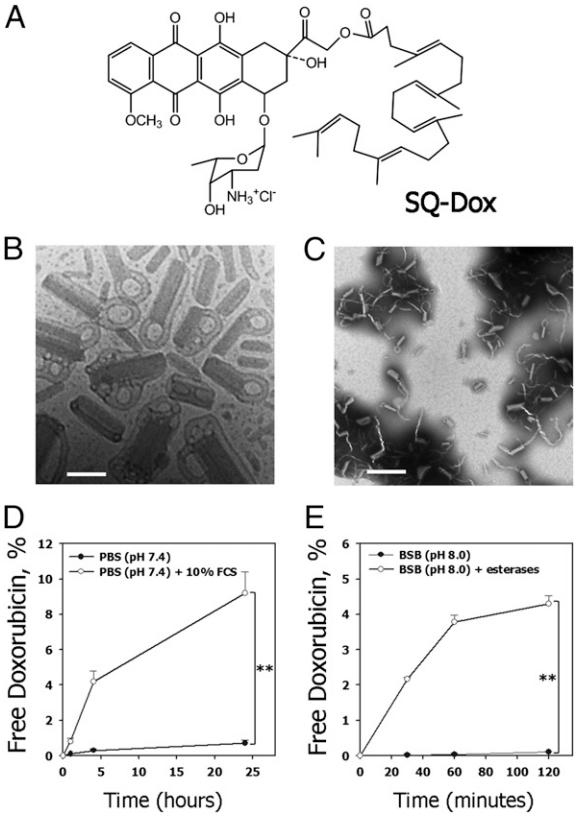

Fig. 1. Nanoassemblies of the squalenoyl prodrug of doxorubicin (SQ-Dox NAs). (*A*) Chemical structure of SQ-Dox. (*B*) Cryo-TEM appearance of the SQ-Dox NAs. (Scale bar, 100 nm.) (*C*) TEM appearance of the SQ-Dox NAs. (Scale bar, 500 nm.) (*D*) Time course of doxorubicin release at 37 °C in PBS (pH 7.4) solution containing 10% FCS ($n = 3$, $^{**}P < 0.01$). (*E*) Time course of doxorubicin release at 37 °C in borate (BSB, pH 8.0) solution containing 25 U/mL esterases ($n = 3$, $^{**}P < 0.01$). Released doxorubicin was separated from the SQ-Dox NAs by centrifugation and quantified using HPLC (for experimental details, see *SI Materials and Methods*).

nanoassemblies, and subsequent removal of the organic solvent by evaporation resulted in pure nanosuspension. By modifying the respective volumes of THF and aqueous phase, the concentration of the SQ-Dox, as well as the ionic strength of the water phase, it was possible to select the optimal suspension containing nanoassemblies of 130-nm mean diameter with narrow particle size distribution (PSD < 0.2, as measured by quasielastic light scattering) and a positive ζ-potential (+35.5 mV). The size, size distribution, and ζ-potential of the nanoassemblies were reproducible, with three independent preparations giving nearly identical results for each sample. The drug loading of SQ-Dox nanoassemblies (NAs) was calculated (ratio between molecular weights in percent) to be 57%. When characterized by transmission electron microscopy (TEM) or cryogenic-transmission electron microscopy (cryo-TEM), SQ-Dox nanoassemblies displayed a mixture of "loop-train," "rod," and "head-tail" original structures, as shown in Fig. 1*B* (cryo-TEM) and Fig. 1*C* (TEM). The nanosuspension showed excellent physical and chemical stability during storage for 6 months (at 4 °C in the dark) (Fig. S2), whereas sensitivity to increased ionic strength and to the type of counter ions was observed (Tables S1–S5). For this reason, SQ-Dox NAs were used as a suspension in water when no other precision was given.

Incubation of SQ-Dox NAs in PBS containing 10% (vol/vol) FCS has evidenced a slow release of doxorubicin (Fig. 1*D*). After 24 h of incubation, ~9% of the total drug content was found

liberated from SQ-Dox NAs in the presence of serum, whereas only 0.6% was released in the absence of serum. To further investigate if the doxorubicin release from SQ-Dox NAs resulted from the enzymatic hydrolysis of the prodrug (likely at the level of the ester linkage), an additional release experiment was performed in an esterase containing buffer solution, according to the standard protocol provided by the manufacturer, as described in *SI Materials and Methods* (Fig. 1*E* and Fig. S3). After 2 h of incubation, ~4% of the total drug content was released from SQ-Dox NAs in the presence of esterases, compared with only 0.1% in the absence of esterases.

In Vitro Cell Uptake and Antitumor Activity. To investigate the mechanism of drug uptake into cells, free doxorubicin or SQ-Dox NAs were incubated with a human pancreatic carcinoma cell line (MiaPaCa-2) and the cell internalization was monitored by fluorescence microscopy (10 μM) and flow cytometry (1 μM). The cell penetration of SQ-Dox NAs was faster and the intracellular drug concentration remained greater than native doxorubicin (Fig. 2*E*). As clearly shown in Fig. 2*A*, SQ-Dox NAs (red) rapidly localized into the cell cytoplasm (phalloïdine-FITC, green staining) and nucleus (DAPI, blue staining) as early as 5 min postincubation. After 4 h, the cell uptake of SQ-Dox NAs was three-times more important than that of free doxorubicin, with major localization in the cytoplasm (Fig. 2 *B* and *E*). After 24 h, both SQ-Dox NAs and free doxorubicin were observed to produce an intense staining only into the nucleus (Fig. 2 *C* and *E*). When the cells were incubated with SQ-Dox NAs (1 μM) for 4 h at 4 °C (instead of 37 °C), the cell fluorescence intensity dramatically decreased (Fig. 2*F*), suggesting endocytosis as the major pathway of cell internalization of SQ-Dox NAs.

We further examined the antitumor efficacy of SQ-Dox NAs on the growth of MiaPaCa-2 cell line as per the methodology described in the *SI Materials and Methods*. Incubation (72 h) with SQ-Dox NAs has reduced the cell proliferation in a concentration-dependent manner (Fig. S4*A*). Although free doxorubicin displayed a slightly better antiproliferative effect than SQ-Dox NAs (IC_{50} was 90 and 180 nM, respectively), a much more efficient suppression of the malignant tumor cell invasion was observed with SQ-Dox NAs, assessed using the migration assay (Fig. S4 *B* and *C*). Total suppression of MiaPaCa-2 cell invasion was, indeed, only observed after SQ-Dox NA treatment at IC_{50} concentration. To further confirm the doxorubicin-induced apoptosis, MiaPaCa-2 cells were treated with SQ-Dox NAs at IC_{50} and IC_{10} concentrations (180 nM and 70 nM, respectively) and compared with free doxorubicin (90 nM and 10 nM, respectively). After 72 h of incubation, Annexin-V and propidium iodide staining of the cells revealed a higher induction of apoptosis in SQ-Dox NA-treated cells compared with the doxorubicin-treated cells (Fig. 3*B*). Indeed, treatment of the cells with SQ-Dox NAs at IC_{50} concentration for 72 h resulted in 50% of cells in the apoptosis phase ($P < 0.01$); more precisely, ~40% of cells were in the early apoptosis phase and ~4% cells in the late apoptosis phase, whereas treatment with free doxorubicin resulted in only 10% of cells in the apoptosis phase (either early or late apoptosis phase). The difference was still more pronounced at IC_{10} concentrations, where the SQ-Dox NA treatment led to 80% of cells in the early apoptosis phase compared with only 7% of the cells in this phase with native doxorubicin treatment. To further confirm these effects, we analyzed poly(ADP-ribose) polymerase (PARP) and caspase-3 activation, a hallmark of the apoptosis induction (29). SQ-Dox NA treatment induced an increased caspase-3 activity (Fig. 3*A*) and cleavage of PARP (Fig. 3*C*), compared to the untreated controls, suggesting that the antiproliferative and cytotoxic effects of SQ-Dox NAs could be attributed, at least in part, to the activity of these apoptosis mediators. However, caspase-3 activity ($P < 0.01$) and PARP cleavage were still more important with free doxorubicin, which may be explained by the slow- and long-lasting release of the parent drug from SQ-Dox NAs, as already shown in Fig. 1*D*.

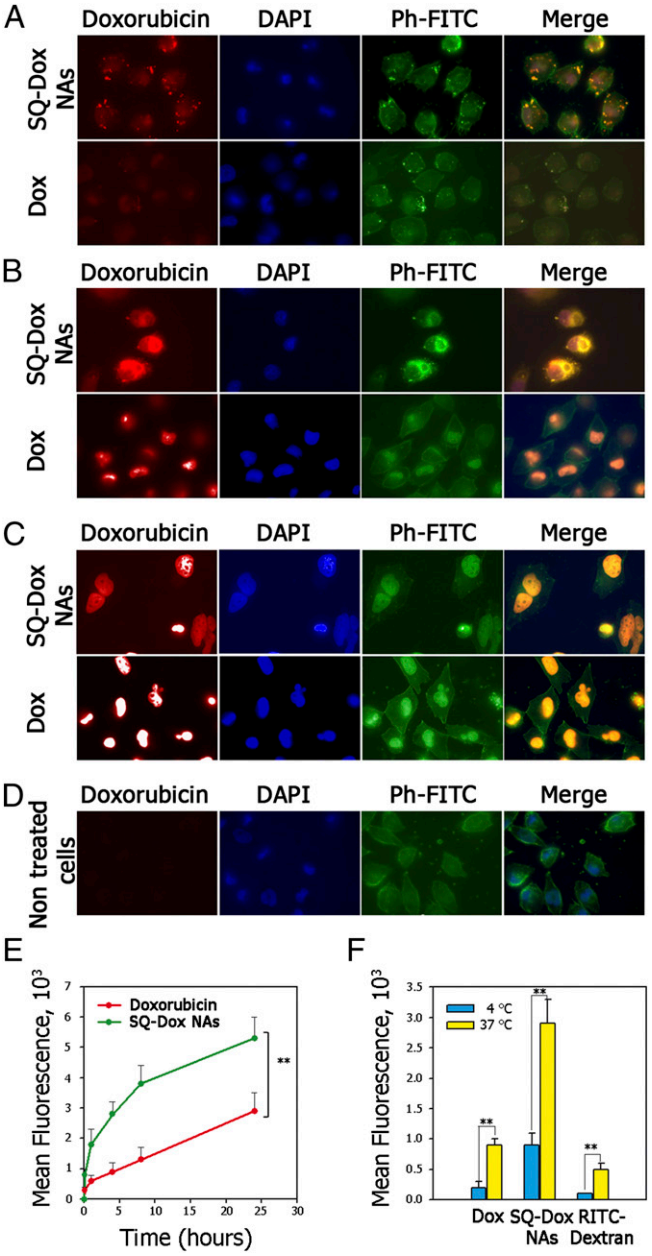

Fig. 2. Cell internalization of free doxorubicin and SQ-Dox NAs. (*A–C*) Fluorescence microscopy images of MiaPaCa-2 cells show the cellular uptake of free doxorubicin or SQ-Dox NAs (concentration of 10 μM) at 5 min (*A*), 4 h (*B*), and 24 h (*C*). (*D*) Nontreated cells. The nuclei were stained with DAPI, FITC-conjugated phalloïdine was used to label F-actin, and (last column) overlay of all types of staining. All cells (*A–D*) were imaged using a fluorescence microscope (Leica) with a 40× oil-immersion objective. (*E*) Time course of doxorubicin (red) accumulation into the cells exposed to 1 μM free doxorubicin or SQ-Dox NAs as measured using flow cytometry ($n = 3$, $^{**}P < 0.01$). (*F*) Doxorubicin fluorescence in the cells after 4 h of exposure to 1 μM free drug or SQ-Dox NAs at 4 °C and 37 °C ($n = 3$, $^{**}P < 0.01$). RITC-Dextran was used as a positive control of endocytosis. Results are reported as means ± SD.

Overall Toxicity. The systemic toxicity of SQ-Dox NAs has been first investigated, compared to free doxorubicin or to its liposomal formulations (Myocet and Caelyx), by determining the maximum tolerated dose (MTD) after single or repeated intravenous injection

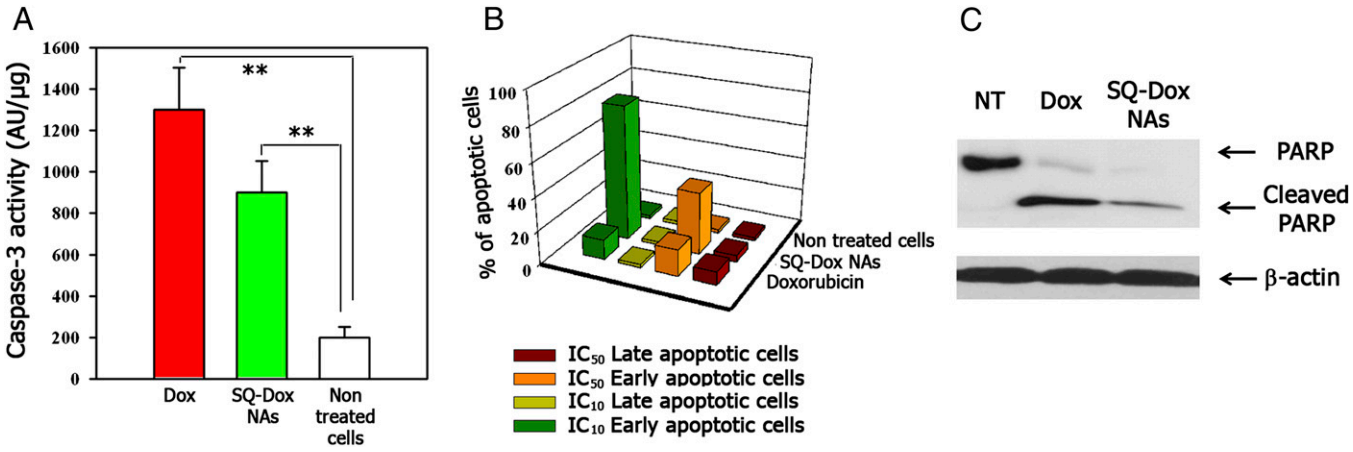

Fig. 3. In vitro antitumor activity of SQ-Dox NAs. (*A*) Caspase-3 activity. Data are expressed in arbitrary units per microgram of protein, and the results are the representative of two independent experiments performed in triplicate (**$P < 0.01$). (*B*) Evaluation of apoptosis induced by doxorubicin and SQ-Dox NAs. MiaPaCa-2 cancer cells were incubated with SQ-Dox NAs or free doxorubicin at IC_{50} and IC_{10} concentrations (IC_{50} was 90 and 180 nM, and IC_{10} was 10 and 70 nM for doxorubicin and SQ-Dox NAs, respectively). The percentages of apoptotic cells were significantly different between SQ-Dox NAs and the free-doxorubicin treatments. (*C*) Western blot analysis performed using antibodies specific to PARP. β-Actin was used as a loading control.

to the female nude or CD2F1 mice. The MTD was estimated based on the threshold at which all of the animals survived with a body-weight loss of less than 10%. Whatever the dosing protocol, the MTD of SQ-Dox NAs was found to be up to fivefold higher than that of free doxorubicin or Myocet, and up to threefold higher than that of Caelyx after intravenous administration (Table S6). Concerning the local toxicity, it has been observed that the free doxorubicin at a dose of 6 mg/kg induced dramatic necrosis at the site of injection, but such necrosis has not been observed with SQ-Dox NAs at dose as high as 20 mg/kg, equivalent doxorubicin.

Cardiac Toxicity. Cardiac toxicity, the main toxicological target of doxorubicin, was investigated in the standard experimental model of hypertensive rats (10) injected weekly, either with 1 mg·kg·wk of free doxorubicin or with SQ-Dox NAs at a dose of 1 or 2 mg·kg·wk (equivalent doxorubicin). Under these experimental conditions, the toxicity of free doxorubicin translated into mortality of four of eight rats; the death occurred between day 63 and day 76 (Fig. S5*A*). In this group, clinical signs noted before death were lessened handling reactivity compared with the saline-treated rats, and the appearance of necrosis at the site of injection (in four rats). Regarding the body weight and food consumption, the signs of toxicity appeared in the doxorubicin-treated animals starting from the fifth week, at which time the animals started to lose weight, accompanied by a statistically significant decrease in food consumption (Fig. S5 *B* and *C*). From the ninth dosing (i.e., day 61), the tendency of a decrease in water consumption appeared. In the four surviving rats killed at day 78, the discoloration of the kidneys has been observed. Although the weight of the hearts of the doxorubicin-treated rats was similar to that of the controls or of the SQ-Dox NA-treated rats (Fig. S5*D*), the histological analysis of the cardiac tissues revealed drastic myocardial lesions with important cell vacuolization (Fig. 4*C*). In rats injected with SQ-Dox NAs at 1 and 2 mg·kg·wk equivalent doxorubicin (Fig. 4 *B* and *D*), neither mortality nor any clinical signs of toxicity were noted throughout the whole study. Histological examinations did not show any myocardial lesions in the group of rats treated with SQ-Dox NAs at 1 mg·kg·wk (equivalent doxorubicin) (Fig. 4*B*). Only a slight incidence of minimal myocardiopathology has been observed after treatment with SQ-Dox NAs at 2 mg·kg·wk (Fig. 4*D*).

Concerning the serum troponin-T levels, a marker of cardiac myocyte injury (30), a dramatic increase was measured from day 42 in animals dosed with free doxorubicin at 1 mg/kg (Fig. 4*E*). In this group of animals, troponin-T concentration reached a plateau from day 70. In animals dosed with SQ-Dox NAs at 1 and 2 mg·kg·wk (equivalent doxorubicin), the troponin-T levels remained similar to those of the control groups. As a whole, these data evidenced that even at a dose double than that of the parent drug, the cardiotoxicity of SQ-Dox NAs was dramatically low comparatively to free doxorubicin.

Antitumor Activity in Subcutaneous Tumor Xenograft Models. The anticancer activity of SQ-Dox NAs was tested using xenograft models of human pancreatic and murine lung cancers developed by the injection of MiaPaCa-2 cells or M109 cells in the flank of athymic nude or CD2F1 mice, respectively. After tumors had grown to 80–100 mm^3, the animals were divided into four groups in such a manner as to minimize the weight and the tumor-size differences among the groups. Based on the MTD previously determined (i.e., 15 mg/kg per injection, equivalent doxorubicin for SQ-Dox NAs and 3 mg/kg per injection for free doxorubicin), the following treatments and doses were administered by intravenous injections in the lateral tail vein on days 0, 4, 8, 12, and 16: (*i*) saline, (*ii*) squalenic acid nanoassemblies (SQCOOH NAs, 100 mg/kg), (*iii*) free drug (3 mg/kg), and (*iv*) SQ-Dox NAs (15 mg/kg, equivalent doxorubicin). As indicated in Fig. 5, the growth of MiaPaCa-2 (Fig. 5*A*) and M109 (Fig. 5*C*) tumors were not affected by the treatment with squalenic acid nanoassemblies, compared with the saline-treated tumors. The treatment with free doxorubicin reduced the volume of MiaPaCa-2 tumors by only 29% ($P < 0.01$), but had no effect on the growth of M109 tumors. At the same time, mice treated with SQ-Dox NAs showed a more drastic tumor growth inhibition of 95% for MiaPaCa-2 and of 90% for M109 ($P < 0.01$) tumors. The absolute weight-loss differences in the native doxorubicin and SQ-Dox NA-treated groups were modest at the doses studied in mice bearing subcutaneous MiaPaCa-2 xenografts (Fig. 5*B*). In contrast, a drastic weight loss was observed in the free doxorubicin-treated mice bearing subcutaneously engrafted M109 tumors (20%) (Fig. 5*D*), whereas no weight decrease was observed after SQ-Dox NA treatment.

In an additional experiment, the anticancer activity of SQ-Dox NAs was compared with long-circulating liposomal formulations of doxorubicin (Myocet and Caelyx) using the same xenograft model of human pancreatic cancer. As indicated in Fig. 5*E*, the treatment with Myocet or Caelyx (at MTD) reduced the volume of MiaPaCa-2 tumors by 50% and 58% ($P < 0.01$), respectively,

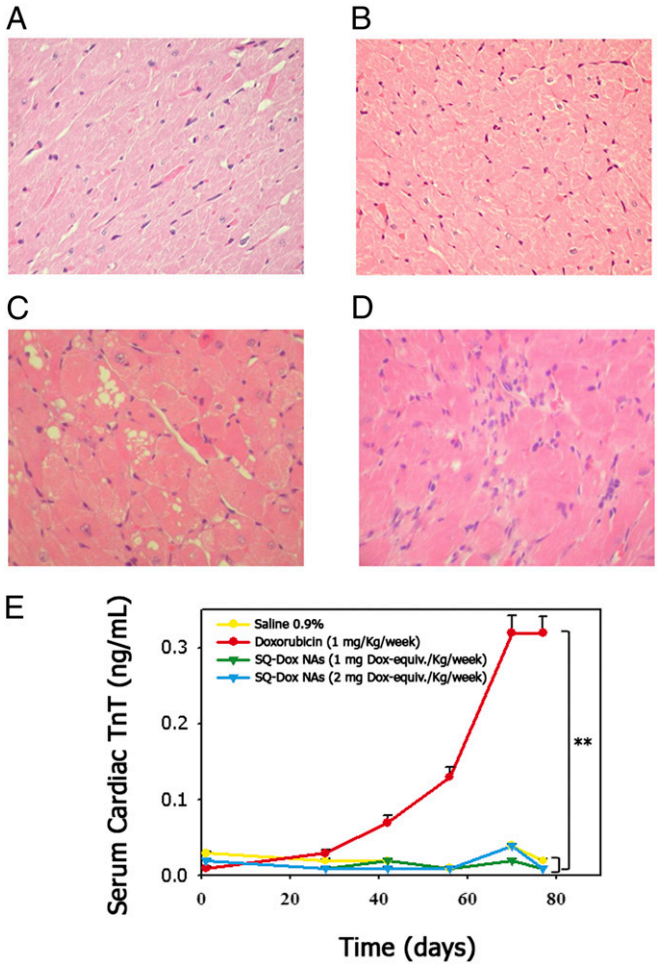

Fig. 4. Evaluation of the cardiotoxicity induced by doxorubicin. (*A–D*) HES-stained sections of cardiac tissue (left ventricular inner myocardium) of SH male rats. All tissue images (*A–D*) were analyzed by microscopy at 100× magnification (Leica). (*A*) Saline-treated rat showing myocardium without any lesions (no ventricle focal inflammatory cell). (*B*) SQ-Dox NA-treated rat (dose: 1 mg·kg·wk equivalent doxorubicin, during 11 wk) showing myocardium without any lesions. (*C*) Doxorubicin-treated rat (dose: 1 mg·kg·wk, during 11 wk) showing infiltration with ventricle hypercellularity. (*D*) SQ-Dox NA-treated rat (dose: 2 mg·kg·wk equivalent doxorubicin, during 11 wk) showing myocardium without any lesion, only a slight incidence of minimal myocardiopathology was observed. (*E*) Time course of serum concentrations of cardiac troponin-T (TnT) in hypertensive rats injected weekly during 11 wk with either 1 mg·kg·wk of doxorubicin or with 1 or 2 mg·kg·wk (equivalent doxorubicin) of SQ-Dox NAs (**$P < 0.01$ vs. doxorubicin and $P > 0.1$ vs. saline treated rat; $n = 8$).

compared with the saline-treated tumors (day 18). It should be noted that a significant weight loss was observed in Caelyx-treated mice (10–15%) at day 18, which was the expression of drug's toxicity (Fig. 5*F*). At the same time, mice treated with SQ-Dox NAs showed a more drastic tumor-growth inhibition of 86% at day 18 ($P < 0.01$) (Fig. 5*E*) without any weight loss (Fig. 5*F*), thus demonstrating the superiority of SQ-Dox NAs.

In a nutshell, the squalenoylation of doxorubicin allowed delivering larger doses of drug without observable toxicity, thus improving the efficacy and drug's therapeutic index.

Immunohistochemical Evaluation of Antitumor Activity of SQ-Dox NAs in Tumor Xenografts. Immunohistochemical analysis of the biopsies obtained from the SQ-Dox NA-treated tumor tissues in mice bearing subcutaneously engrafted M109 xenografts (Fig. 6*A*) demonstrated enlarged cells with significant necrotic changes. Drastic suppression and replacement of the tumor cells by normal tissue has been also observed (Fig. 6*A* and Fig. S6*A*). Apoptosis analysis revealed that the TUNEL$^+$ cells were more prominent in M109 tumor biopsies obtained from mice treated with SQ-Dox NAs (Fig. 6 *A* and *C*). Immunostaining of the active form of caspase-3 protease (29) revealed a more marked caspase-3 activity in SQ-Dox NA-treated mice, compared with the free

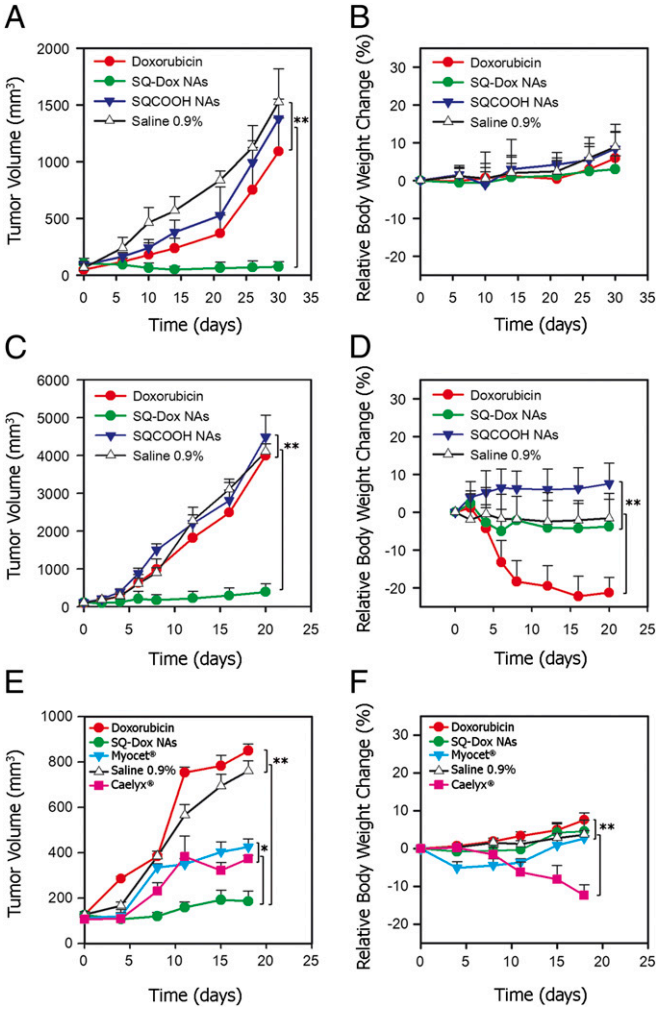

Fig. 5. Anti-tumor activity of SQ-Dox NAs. (*A–D*) Tumor growth inhibition by SQ-Dox NAs and the body-weight changes of mice bearing MiaPaCa-2 (*A* and *B*) or M109 (*C* and *D*) tumors. Tumor volume (*A* and *C*) and body weight (*B* and *D*) were regularly measured during the experimental period ($n = 10$, **$P < 0.01$). The mice were injected with doxorubicin (5 × 3 mg/kg, MTD), SQ-Dox NAs (5 × 15 mg/kg equivalent doxorubicin, MTD), saline 0.9%, or SQCOOH NAs (100 mg/kg). All groups ($n = 10$) of mice received these treatments on days 0, 4, 8, 12, and 16 by intravenous injection in the lateral tail vein (10 μL/g of the body weight). Results are reported as means ± SD. (*E* and *F*) Comparison of the antitumor activity and toxicity of SQ-Dox NAs with liposomal formulations of doxorubicin (Myocet and Caelyx) administered in nude mice bearing subcutaneous engrafted MiaPaCa-2 tumors. The mice were injected with doxorubicin (5 × 3 mg/kg, MTD), SQ-Dox NAs (5 × 15 mg/kg equivalent doxorubicin, MTD), liposomal formulation of doxorubicin (Myocet, 5 × 3 mg/kg equivalent doxorubicin, MTD), PEGylated liposomal formulation of doxorubicin (Caelyx, 5 × 5 mg/kg equivalent doxorubicin, MTD), and saline 0.9%. All groups ($n = 6$) of mice received these treatments on days 0, 4, 8, 11, and 15 by intravenous injection in the lateral tail vein (10 μL/g of the body weight). Tumor volume (*E*) and body weight (*F*) were regularly measured during the experimental period ($n = 6$, *$P < 0.05$, **$P < 0.01$). Results are reported as means ± SD.

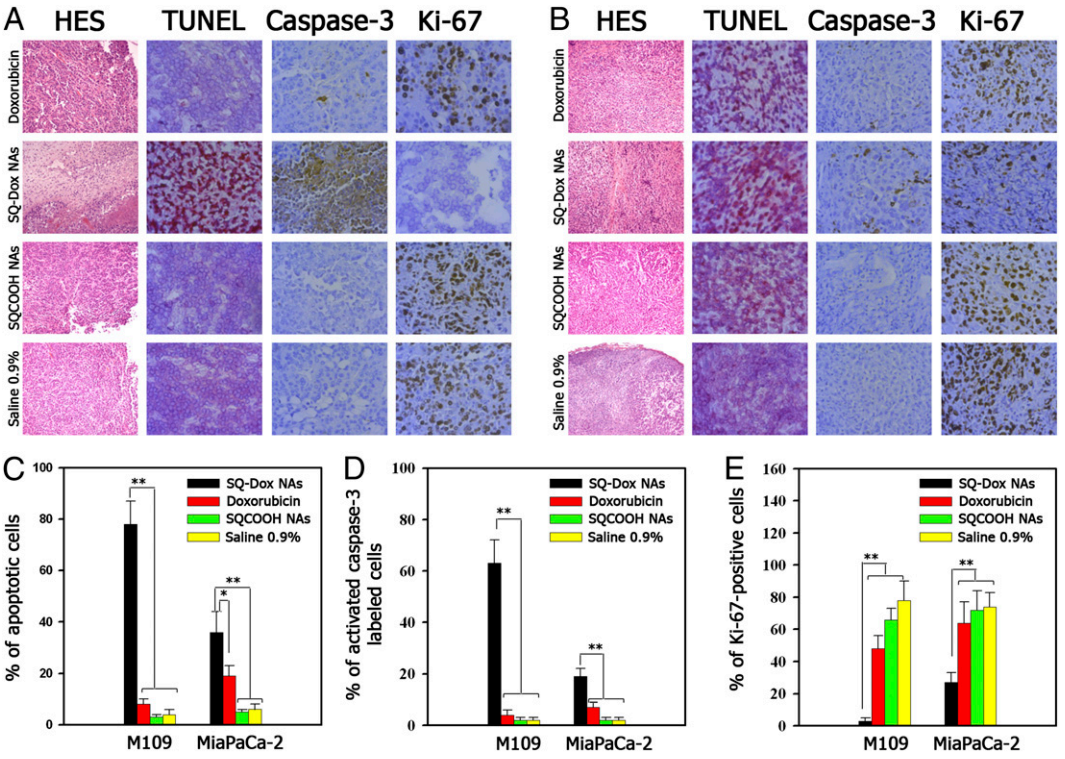

Fig. 6. Immunohistochemical staining of the tumor tissues derived from injected M109 (*A*) murine lung and MiaPaCa-2 (*B*) human pancreatic cancer cells. The tumors were treated by (*i*) SQ-Dox NAs (5 × 15 mg/kg, equivalent doxorubicin, MTD), (*ii*) doxorubicin (Dox, 5 × 3 mg/kg, MTD), (*iii*) saline (0.9%), or (*iv*) SQCOOH NAs (5 × 100 mg/kg), and excised at day 16. Paraffin sections from tumor biopsies were submitted to HES (*Left*), TUNEL (*Center Left*), caspase-3 (*Center Right*), and K_i-67 (*Right*) staining. HES/M109/SQ-Dox NAs: inflammatory tissue without carcinomatous cells (*Upper* field), necrotic tumor with a few dystrophic carcinomatous nuclei (*Lower* field); HES/M109/doxorubicin or SQCOOH NAs, or saline: viable carcinomatous cells. HES/MiaPaCa-2/SQ-Dox NAs: well preserved carcinomatous cells (*Left*), major fibrosis with degenerative tumor cells (*Right*); HES/MiaPaCa-2/doxorubicin or SQCOOH NAs, or saline 0.9%: viable carcinomatous cells, absence of fibrosis. (*C*) Quantification of the TUNEL assay showed significantly increased apoptosis ($n = 5$, $^*P < 0.05$, $^{**}P < 0.01$) in the tumors from SQ-Dox NA-treated mice (vs. doxorubicin, SQCOOH nanoassemblies, or saline-treated mice). (*D*) The counts of activated caspase-3 labeled cells showed significantly increased labeling in the tumors from SQ-Dox NA-injected animals (vs. doxorubicin, SQCOOH NA- or saline-treated mice) ($n = 5$, $^{**}P < 0.01$). (*E*) A lower number of proliferating cells was observed in counts of K_i-67$^+$ cells in the tumor tissue sections of mice receiving SQ-Dox NA therapy (vs. doxorubicin, SQCOOH NAs or saline-treated mice) ($n = 5$, $^{**}P < 0.01$). Results are reported as the mean ± SD.

doxorubicin-treated mice (Fig. 6 *A* and *D*). Additionally, SQ-Dox NAs caused a considerable decrease of the M109 tumor proliferative activity, comparatively to the parent drug, as indicated by the reduced number of K_i-67$^+$ tumor cells (Fig. 6 *A* and *E*). Similar observations concerning the apoptotic activity of SQ-Dox NAs were made with MiaPaCa-2 tumor model (Fig. 6 *B*–*E*).

Tissue Distribution and Pharmacokinetics Studies. To explain the higher anticancer activity and lower toxicity of SQ-Dox NAs vs. free doxorubicin, we performed pharmacokinetics and biodistribution studies in nude mice. Bioavailability, calculated from the area under the blood concentration vs. time curve from 0 to 24 h ($AUC_{0–24}$), was compared for SQ-Dox NAs and the free drug. After administration of SQ-Dox NAs, the $AUC_{0–24}$ of doxorubicin in blood was 4.4-times higher than after injection of free doxorubicin (mean = 184 vs. 42 μg·h·mL, difference = 142 μg·h·mL) (Fig. 7*A*). In parallel, the urinary excretion of doxorubicin was found dramatically reduced in SQ-Dox NA-treated mice (Fig. 7*C*), demonstrating that the SQ-Dox NAs significantly increased the body longevity of doxorubicin.

Concerning the tissue distribution, at 24 h postinjection, SQ-Dox NAs led to a 2.5-fold increase of the concentration of doxorubicin in MiaPaCa-2 tumor, compared to the free doxorubicin treatment (Fig. 7*D*), whereas the concentration of doxorubicin at several nontumor sites in the body, including the lungs, kidneys (Table S7), and heart (Fig. 7*B*) was found diminished. Concerning the cardiac tissue, the toxicity of which represents the dose-limiting side effect of doxorubicin (31), the SQ-Dox nanomedicine was found to notably decrease the peak concentration of the native drug, compared to free doxorubicin (by 15- and 4-fold, respectively, at 2 h and 24 h posttreatment, $P < 0.01$) (Fig. 7*B*).

Discussion

Doxorubicin is a highly potent antitumor agent that is among one of the most active antineoplastic drugs developed to date (see funding sources, refs. 7–9). However, its clinical application is limited by cardiac hypertrophy, a dose-limiting side effect arising from the formation of free-radicals and lipid peroxidation (32). The design of doxorubicin-loaded nanocarriers (i.e., liposomes or nanoparticles) has gained increasing interest as a mean of improving the treatment of neoplastic diseases and reducing the drug-mediated cardiotoxicity (16, 33–35). However, the need to surface-functionalize these nanodevices with PEG raises toxicological issues because of the previously mentioned biodegradability and safety concerns of PEG (23, 36). In this context, we have identified that the linkage of doxorubicin to the natural lipid squalene allowed, through a simple manufacturing procedure, the construction of nanoassemblies of 130 nm with impressively high drug loading (i.e., 57%), slow drug release, and display of an original loop-tail elongated structure never observed before. The reason for this surprising self-assembled nanoconstruction deserves further physico-chemical and morphological investigations, but it is likely that, as discussed below, the elongated morphology would be responsible for the observed long-circulating properties of SQ-Dox.

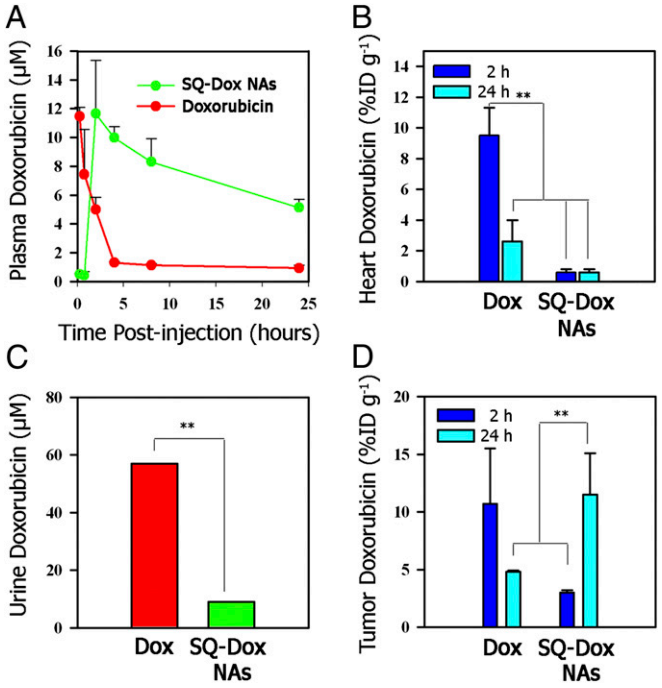

Fig. 7. Plasma pharmacokinetics and tissue biodistribution. (*A*) Plasma doxorubicin concentrations resulting from a single injection of SQ-Dox NAs (8 mg/kg equivalent doxorubicin) or free doxorubicin (8 mg/kg, MTD), as a function of time postinjection. The values are the mean ± SD (n = 3–4). (*B*) Cardiac concentration of doxorubicin, 2 h and 24 h after a single injection of either SQ-DOX NAs (8 mg/kg, equivalent doxorubicin) or free doxorubicin (8 mg/kg) (n = 3–4, $^{**}P < 0.01$). (*C*) Urine doxorubicin concentrations, 24 h after administration of a single injection of SQ-Dox NAs (8 mg/kg equivalent doxorubicin) or free doxorubicin (8 mg/kg, MTD) ($^{**}P < 0.01$). Urine was collected in metabolic cages (five mice per cage) and doxorubicin concentrations were measured as described in *Materials and Methods*. (*D*) Tumor concentrations of doxorubicin, 2 h and 24 h after a single injection of either SQ-DOX NAs (8 mg/kg, equivalent doxorubicin) or free doxorubicin (8 mg/kg) (n = 3–4, $^{**}P < 0.01$). The values are the mean ± SD.

On the other hand, the SQ-Dox NAs demonstrated high stability in the media studied, with less than 1% of the conjugate being hydrolyzed after 24 h. The release of doxorubicin from the bioconjugate following incubation in serum or in esterase-containing buffer was attributed to the enzymatic hydrolysis of the SQ-Dox prodrug.

The antitumor efficacy of this unique doxorubicin nanoformulation has been investigated on human pancreatic (MiaPaCa-2) and murine lung (M109) carcinomas as models of more common and aggressive diseases. These experimental models were chosen because they are very difficult to cure and are resistant to native doxorubicin. For example, it was reported that a potent derivative of doxorubicin (2-pyrrolino-doxorubicin, AN201) and its cytotoxic somatostatin analog (AN-238) targeted to somatostatin receptor subtypes 5 and 3 were not active on MiaPaCa-2 after multiple administration (37). Interestingly, we found that the uptake into MiaPaCa-2 cells of these SQ-Dox NAs occurred very rapidly (as early as 5-min postincubation) and was increased comparatively to free doxorubicin. The internalization into cells was thought to occur via endocytosis with early endosomal localization, rapidly followed by a more homogeneous diffusion of doxorubicin's fluorescence into the cell cytoplasm, probably because of the intracellular release of the drug from SQ-Dox NAs. Further diffusion of the drug into the nucleus allows an efficient induction of cell apoptosis (better than the parent drug, both at IC_{10} and IC_{50} concentrations).

In vivo toxicity studies have shown that the MTD of SQ-Dox NAs was up to fivefold higher than the free doxorubicin after intravenous administration. A specific cardiotoxicity investigation performed on hypertensive rats has shown that the SQ-Dox NAs did not cause any myocardial lesions, such as those observed after the free-doxorubicin treatment. This finding may be explained by the lower cardiac concentration of the drug after SQ-Dox NA administration, as evidenced in the biodistribution study. Concerning the pharmacological activity, SQ-Dox NAs have shown a higher antitumor efficacy on both MiaPaCa-2 and M109 tumor xenografts, compared to free doxorubicin. Remarkably, the tumor growth inhibition was 90% by SQ-Dox NAs against only 3% by the free doxorubicin on M109 tumors, strongly demonstrating the ability of this squalenoyl nanomedicine to cure the doxorubicin-resistant cancer. It should be noted that SQ-Dox NAs also displayed a lower toxicity and a better anticancer activity than Caelyx and Myocet, the two doxorubicin liposomal formulations currently on the market. Because resistance to apoptosis is one of the hallmarks of cancer, we further evaluated the mechanism of cell death in tumor biopsy samples. The tumors from the mice treated with SQ-Dox NAs presented an increased number of apoptotic cells (vs. the tumors from the mice treated with free doxorubicin) as determined by TUNEL analysis and an augmented staining of caspase-3. Moreover, the data from the K_i-67 test of tumor sections from the mice receiving SQ-Dox NA therapy (vs. doxorubicin- or saline-treated mice) clearly revealed the efficacy of SQ-Dox NAs in eliminating the proliferating tumor cells from the tumor tissue.

Such increased anticancer activity of SQ-Dox NAs may be explained by the pharmacokinetic and biodistribution data. Indeed, the squalenoyl doxorubicin nanomedicine: (*i*) significantly increased the accumulation of the drug into the tumor, compared to the free doxorubicin (i.e., by 2.5-fold at 24 h after administration); (*ii*) induced blood longevity of the drug; and (*iii*) decreased the urinary excretion of the drug. The prolonged circulation time of SQ-Dox NAs in the bloodstream and their ability to evade clearance mechanisms may be explained by the more elongated morphology of SQ-Dox NAs, compared to the other colloids usually displaying a more spherical shape. Indeed, worm-like micelles (filomicelles) formulated from an amphiphilic diblock copolymer, poly(ethylene oxide)-b-poly(e-caprolactone), have shown unprecedented prolonged circulation times in rodents, considerably longer than for spherical particles of the same copolymer (38, 39). Long flexible filomicelles were extended by the flow along streamlines, which tended to oppose interactions with phagocytes (and capillary walls). In contrast, these filomicelles were able to enter cells under static conditions.

We demonstrated here that even if a drug has no relevant indication for a given experimental cancer (which is the case of doxorubicin for the experimental human pancreatic cancer MiaPaCa-2), the drug can be made efficient using the nanotechnology strategy described in this article. This approach is expected to open interesting therapeutic prospects in oncology. Of note, the approach described herein was also found to be applicable to paclitaxel, another anticancer compound with hydrophobic properties. When conjugated to squalene (Fig. S7), this compound self-assembled as nanoparticles, displaying in vivo a comparable anticancer activity than paclitaxel-Cremophor EL but with a dramatically lower systemic toxicity (more than three times) (Figs. S8 and S9), whereas in vitro cytotoxicity was dramatically reduced (Table S8).

The data shown in this article strongly suggest the candidature of the squalenoylated doxorubicin nanomedicine described herein for clinical assessment in human cancers, for which the current treatment using doxorubicin is limited by its toxicity. Interesting prospects may also be considered for the treatment of pancreatic cancers.

Materials and Methods

Cell Culture. Murine lung carcinoma cell line M109 and human pancreatic cancer cell line MiaPaCa-2 were obtained from the American Type Culture Collection and maintained as recommended. Briefly, M109 cells were maintained in RPMI medium 1640. MiaPaCa-2 cells were grown in DMEM-glutamine medium. Media were supplemented with 10% heat-inactivated FCS, penicillin (100 U/mL), and streptomycin (100 μg/mL). The cells were maintained in a humid atmosphere at 37 °C with 5% CO_2.

Synthesis, Preparation, and Characterization of SQ-Dox NAs. Doxorubicin-14-squalenate (SQ-Dox) was synthesized by esterification of 14-bromodaunorubicin HCl (prepared by bromination of daunorubicin HCl) with 1,1′,2-Tris-norsqualenoic acid in the presence of potassium carbonate, as detailed in *SI Materials and Methods*. SQ-Dox NAs were prepared using the nanoprecipitation method after optimization as indicated in *SI Materials and Methods* and the best formulation was used for further in vitro and in vivo studies. Briefly, 500 μL of the tetrahydrofuran solution of SQ-Dox (4 mg/mL) was added drop-wise under stirring (500 rpm) into 1 mL distilled water. Precipitation of the SQ-Dox NAs occurred spontaneously. THF was completely evaporated using a Rotavapor at 20 °C under vacuum to obtain an aqueous suspension of pure SQ-Dox NAs (final concentration 2 mg/mL). Nanoassemblies made of squalenic acid alone were prepared in a similar manner. The final concentration of the aqueous suspension of squalenic acid was 2 mg/mL. The morphology of the SQ-Dox NAs was examined using a TEM and cryo-TEM (for experimental details, see *SI Materials and Methods*). The release of doxorubicin from the SQ-Dox NAs was investigated after incubation in PBS with or without serum and in borate buffer in the presence and in the absence of esterases. For details, see *SI Materials and Methods*.

Study of Doxorubicin Cell Internalization. MiaPaCa-2 cells were cultured on a coverslip in a culture dish for 24 h to achieve ∼40% confluence. Cells were then incubated with free doxorubicin or SQ-Dox NAs at the concentration of 10 μM (37 °C) for different time periods. After treatment, the cells were washed with Dulbecco's PBS, fixed in 3% paraformaldehyde (PFA), stained with phalloïdine-FITC (200 μM) and DAPI (40 μM) (Invitrogen), washed with Dulbecco's PBS five times, and imaged using a fluorescence microscope (Leica) with a 40× oil-immersion objective. The following wavelengths were used: excitation at 488 nm and detection through a 515-nm filter for FITC, and excitation at 488 nm and detection through a 560-nm filter for doxorubicin.

To quantitatively measure the cell internalization of SQ-Dox NAs, MiaPaCa-2 cells were cultured on six-well plates for 24 h to achieve 60–80% confluence. SQ-Dox NAs or the free doxorubicin were then added at the concentration of 1 μM to each well. After incubation, the cells were collected at different time intervals for measurement of doxorubicin fluorescence. To investigate the mechanism of cell internalization, the cells were incubated for 4 h at 4 °C or 37 °C. Rhodamine B-isothiocyanate-conjugated dextran (RITC-Dextran) was used as a positive control of endocytosis. The fluorescence from individual cells was examined using a flow cytometer C6 (Accuri Cytometers). For the fluorescence detection of doxorubicin or RITC-Dextran, the following parameters were used: λ_{ex} = 488 nm and λ_{em} = 560–606 nm. Ten-thousand cells were measured in each sample.

Cell Growth and Apoptosis Assays. MiaPaCa-2 tumor cells were incubated with various concentrations of either SQ-Dox NAs or free doxorubicin for 72 h. After the treatment period, cell viability was measured using a methylthiazoletetrazolium (MTT) method as described in *SI Materials and Methods*. To determine the induction of apoptosis, the Dead Cell Apoptosis Kit (Invitrogen) was used according to the standard protocol provided by the manufacturer, as described in *SI Materials and Methods*.

Western Blot Analysis. MiaPaCa-2 cells were seeded in 75 cm^2 flasks in DMEM containing 10% FCS and cultivated for 24 h before addition of the drug. After incubation for an additional 72 h in the presence of free doxorubicin or SQ-Dox NAs, protein extracts from cells were prepared as described previouisly (40). Equal quantities of protein (50 μg) were resolved on 4–12% NuPage Bis·Tris gradient gels (Invitrogen). Proteins were thereafter transferred to a polyvinylidene difluoride membrane (Millipore). Proteins of interest were identified by reaction with specific primary and secondary antibodies linked to horseradish peroxidase. Briefly, membranes were blocked with 3% BSA in Tris-buffered saline Tween-20 and incubated with rabbit monoclonal antibody to PARP (1/250; Santa-Cruz, Tebu-Bio) overnight at 4 °C. The rabbit monoclonal antibody to β-actin (1/2,000; Santa-Cruz) was used as an internal control for equal gel loading. Immunodetection was performed using horseradish peroxidase-conjugated secondary antibody (Jackson ImmunoResearch) and BM Chemiluminescence Blotting Substrate (PerkinElmer).

In Vivo Study Designs. ***Animals.*** Female CD2F1 and Athymic nude mice were purchased from the Harlan Laboratory. Male spontaneous hypertensive (SH) rats were purchased from Charles River Laboratory. All animals were housed in appropriate animal care facilities during the experimental period, and were handled according to the principles of the laboratory animal care and legislation in force in France. All in vivo studies were performed in accordance with a protocol approved by the Ethical Committee of the Institut Gustave Roussy, France (CEEA IRCIV/IGR 26, registered with the French Ministry of Research).

Determination of the MTD. Six- to 8-wk-old female athymic nude mice and CD2F1 mice were used to evaluate the MTD of a single dose of free doxorubicin or SQ-Dox NAs. Four groups of nude or CD2F1 mice were given a single intravenous injection of free doxorubicin at a dose of 6, 8, 10, or 15 mg/kg and five groups of nude or CD2F1 mice received SQ-Dox NAs at a dose of 8, 10, 15, 17.5, or 20 mg/kg equivalent doxorubicin. The control groups received saline or 100 mg/kg of SQCOOH NAs. MTD was also determined after repeated administration. All groups (n = 4) received five intravenous injections on days 0, 4, 8, 12, and 16 in the lateral tail vein (10 μL/g of body weight). Four groups of nude or CD2F1 mice received free doxorubicin at a dose of 3, 4, 6, or 8 mg/kg and five groups of nude or CD2F1 mice received SQ-Dox NAs at a dose of 8, 10, 15, 17.5, or 20 mg/kg equivalent doxorubicin. The systemic toxicity of liposomal formulations of doxorubicin (Myocet and Caelyx) was also investigated by determining the MTD after single or repeated intravenous injection into female nude mice. Four groups (n = 4) of nude mice were given a single intravenous injection of either Myocet or Caelyx at a dose of 6, 8, 10, or 15 mg/kg and five groups (n = 4) of nude mice received repeated intravenous injection of Myocet or Caelyx at a dose of 3, 5, 8, 10, or 15 mg/kg equivalent doxorubicin on days 0, 4, 8, 11, and 15. The body-weight change and the physical state of mice were monitored for a period of 20 d.

Evaluation of cardiotoxicity. Any possible effect of doxorubicin-induced cardiotoxicity in the case of SQ-Dox NAs was determined comparatively to the free doxorubicin using male SH rats weighing ∼200 g. All of the groups (n = 8) received a weekly intravenous injection for 11 consecutive weeks. One group received free doxorubicin at a dose 1 mg·kg·wk, whereas two other groups received SQ-Dox NAs at a dose of 1 or 2 mg mg·kg·wk equivalent doxorubicin. The control group received 0.9% saline. The injection volume was 1 μL/g for all treated rats. During the course of the study, the rats were observed daily, and the weight, food, and water consumption were measured. Blood samples were collected before the first dosing (day 1), and then once a week after the 4th, 6th, 8th, 10th, and 11th injection, and dispatched for the assessment of serum troponin-T. On the day of necropsy (day 78), the rats were killed by subtotal exsanguinations, and after a macroscopic examination the hearts were removed and weighed. The heart weights of all of the tested rats were similar to that of the control rats. Hearts were then fixed in 4% buffered formalin, paraffin-embedded, and cut into 5-μm-thick sections. Hematoxylin-Eosin-Safran (HES) staining was performed on all specimens of the hearts for histological examinations.

Anticancer efficacy studies. The antitumor efficacy of SQ-Dox NAs was evaluated and compared to free doxorubicin, on the M109- and MiaPaCa-2 tumor-bearing mice. Two-hundred microliters of the cell suspensions, equivalent to 1×10^6 for M109 or 1×10^7 for MiaPaCa-2 cell lines, were injected subcutaneously into CD2F1 or nude mice, respectively, toward the upper portion of the right flank to develop a solid tumor model. Tumors were allowed to grow until a volume of ∼100 mm^3 before initiating the treatment. Tumor length and width were measured using calipers, and the tumor volume was calculated using the following equation: Tumor volume (V) = length × $width^2/2$. Tumor-bearing CD2F1 or nude mice were randomly divided into four groups of 10 each and injected five times with either: (*i*) saline 0.9%, (*ii*) SQCOOH NAs (100 mg/kg), (*iii*) free doxorubicin (3 mg/kg, MTD), or (*iv*) SQ-Dox NAs (15 mg/kg equivalent doxorubicin, MTD). All groups of mice received these treatments on days 0, 4, 8, 12, and 16 by intravenous injection in the lateral tail vein. The injected volume was 10 μL/g of the body weight. The mice were monitored regularly for changes in tumor size and weight.

In another study, and for comparison with liposomal formulations of doxorubicin (i.e., Myocet and Caelyx) (Fig. 5 *E* and *F*), the mice were injected with either doxorubicin (5 × 3 mg/kg, MTD), SQ-Dox NAs (SQ-Dox NAs, 5 × 15 mg/kg equivalent doxorubicin, MTD), liposomal formulation of doxorubicin (Myocet, 5 × 3 mg/kg equivalent doxorubicin, MTD), PEGylated liposomal formulation of doxorubicin (Caelyx, 5 × 5 mg/kg equivalent doxorubicin, MTD), and saline 0.9%. All groups of mice received these treatments on days 0, 4, 8, 11, and 15 by intravenous injection in the lateral tail vein (10 μL/g of

the body weight). The mice were monitored regularly for changes in tumor size and weight.

Immunohistochemical analysis of xenografts. Tumors were excised on day 16, fixed in FineFix (Milestone), paraffin-embedded, and cut into 5-μm-thick sections. HES staining was performed on all of the xenografts for analysis of the morphology. Apoptosis study was performed by caspase-3 staining and TUNEL System (Roche Diagnostics). TUNEL and caspase-3$^+$ cells were analyzed by microscopy (Leica) and counted per view at 40× magnification. Five representative fields were chosen for counting. Necrotic fields were excluded. See more details in *SI Materials and Methods*.

In vivo pharmacokinetics of SQ-Dox NAs. A total of 48 additional healthy nude mice were randomly assigned into two groups (n = 24 mice per group). To measure the pharmacokinetics, SQ-Dox NAs (8 mg/kg equivalent doxorubicin) or free doxorubicin (8 mg/kg, MTD) were intravenously injected into the female nude mice via the tail vein. Blood samples (300 μL) were collected from the tail vein into the heparinized tubes at 15 and 45 min, 2, 4, 8, and 24 h after drug administration (n = 4 at each time point) and then centrifuged (15,000 × g for 10 min at 4 °C) to separate the plasma which was then stored at −70 °C until the doxorubicin measurement.

Biodistribution of SQ-Dox NAs in nude mice. For the biodistribution study, a total of 16 additional nude mice bearing MiaPaCa-2 tumors (diameter 0.5–1 cm) were randomly assigned into two groups (n = 8 mice per group), injected intravenously with either SQ-Dox nanoassemblies (8 mg/kg equivalent doxorubicin) or free doxorubicin (8 mg/kg, MTD). In each treatment group, mice were killed by cervical dislocation at 2 or 24 h after drug administration (n = 4 at each time point). The tumor, spleen, heart, brain, lung, kidney, and liver samples were collected. All tissues were weighed, suspended in 1–3 mL of water (200 mg/mL), and homogenized using 2-mm-diameter zirconium beads (Sigma) for 90 min (25,000 beats per minute). Before and after the homogenization the tissues were kept on ice in the dark. The tissue suspensions were stored at −70 °C until the doxorubicin measurement.

Measurements of doxorubicin in urine. Nude mice (n = 5 per cage) were fed with excess amount of water using a feeding needle and then the urine was collected for 0–24 h in a metabolic cage after a single administration of SQ-Dox NAs (8 mg/kg equivalent doxorubicin) or free doxorubicin (8 mg/kg, MTD). The urine samples were then stored at −70 °C until the doxorubicin measurement.

HPLC analysis of doxorubicin. For HPLC analysis, 100 μL of each plasma or urine sample were spiked with 10 μL of 20 μM idarubicin hydrochloride solution (Internal Standard) before the addition of 500 μL of methanol and centrifugated at 10,000 × g for 10 min at 4 °C. One-hundred microliters of each tissue sample (i.e., tumor, spleen, heart, brain, lung, kidney, and liver) were spiked with 10 μL of 5 μM idarubicin hydrochloride solution (Internal Standard) before addition of 1 mL of a mixture of acetonitrile/methanol [90/10 (vol/vol)], and centrifugated at 15,000 × g for 10 min at 4 °C. Supernatants were then evaporated to dryness under a nitrogen flow at 40 °C and reconstituted in 100 μL of mobile phase [pH 2.5, 0.8% trichloroacetic acid:acetonitrile, 63:37 (vol/vol)]. The extracted drug was quantified by reverse-phase HPLC (Waters) with a C18 column. The system consisted of a Waters 1525 Binary LC pump, a Waters 2707 Autosampler, a C18 Uptisphere column (3 μm, 150 × 4.6 mm; Interchim), HPLC column temperature controllers (model 7950 column heater and chiller; Jones Chromatography) and a Waters 484 programmable fluorescence detector. The HPLC column was maintained at 30 °C. Detection was monitored via doxorubicin intrinsic fluorescence at 570 nm. The mobile phase was delivered at a rate of 1.0 mL/min. The limit of quantitation was 0.05 μg/mL. The data were normalized to the tissue weight. Assuming a 42% hematocrit for blood, the plasma drug concentration was estimated via this standard. Bioavailability from 0 to 24 h (AUC_{0-24}) was calculated from the area under the blood concentration vs. time curve using the linear trapezoidal rule.

Statistical Analysis. All of the data presented in this article are the result of a minimum of three independent experiments. Statistical analyses were performed using Prism GraphPad software. The significance level was calculated using a one-way Anova method, followed by Dunnett's test or with independent Student t test.

ACKNOWLEDGMENTS. We thank Dr. Pierre-Emmanuel Marque for troponin dosage; Miss Olivia Bawa and Dr. Paule Opolon (Institut Gustave Roussy, Villejuif) for analysis of tumors from stained histological slides; Kostantin Chegaev (Dipartimento di Scienza e Tecnologia del Farmaco, Turin, Italy) for generously providing daunorubicin intermediates; the staff of the animal holding facilities (Service Commun Animalerie, Agreement A 92-019-01, Faculté de Pharmacie, Université Paris-Sud 11, France); and Miss Ghislaine Frébourg and Dr. Jean-Pierre Lechaire from the Service de Microscopie Electronique of Institut Fédératif de Recherche (IFR) de Biologie Intégrative (IFR 83) for the Cryo-Transmission Electron Microscopy experiments. This study was supported in part by the European Research Council under the European Community's Seventh Framework Programme FP7/2007-2013 Grant 249835.

1. Drummond DC, Meyer O, Hong K, Kirpotin DB, Papahadjopoulos D (1999) Optimizing liposomes for delivery of chemotherapeutic agents to solid tumors. *Pharmacol Rev* 51(4):691–743.
2. Brannon-Peppas L, Blanchette JO (2004) Nanoparticle and targeted systems for cancer therapy. *Adv Drug Deliv Rev* 56(11):1649–1659.
3. Duncan R (2006) Polymer conjugates as anticancer nanomedicines. *Nat Rev Cancer* 6(9):688–701.
4. Lee CC, MacKay JA, Fréchet JM, Szoka FC (2005) Designing dendrimers for biological applications. *Nat Biotechnol* 23(12):1517–1526.
5. Matsumura Y, Maeda H (1986) A new concept for macromolecular therapeutics in cancer chemotherapy: Mechanism of tumoritropic accumulation of proteins and the antitumor agent smancs. *Cancer Res* 46(12 Pt 1):6387–6392.
6. Couvreur P, et al. (2006) Squalenoyl nanomedicines as potential therapeutics. *Nano Lett* 6(11):2544–2548.
7. American Cancer Society (2011) Doxorubicin. Available at www.cancer.org/Treatment/TreatmentsandSideEffects/GuidetoCancerDrugs/doxorubicin Accessed December 12, 2013.
8. Pfizer Inc. (2011) Doxorubicin Hydrochloride for Injection. Available at http://labeling.pfizer.com/ShowLabeling.aspx?id=530. Accessed December 12, 2013.
9. National Cancer Institute (2013) Cancer Drug Information: Doxorubicin Hydrochloride. Available at www.cancer.gov/cancertopics/druginfo/doxorubicinhydrochloride. Accessed December 12, 2013.
10. Herman EH, el-Hage AN, Ferrans VJ, Ardalan B (1985) Comparison of the severity of the chronic cardiotoxicity produced by doxorubicin in normotensive and hypertensive rats. *Toxicol Appl Pharmacol* 78(2):202–214.
11. Jain A, et al. (2010) Mannosylated solid lipid nanoparticles as vectors for site-specific delivery of an anti-cancer drug. *J Control Release* 148(3):359–367.
12. Liu D, et al. (2011) Drug pH-sensitive release in vitro and targeting ability of polyamidoamine dendrimer complexes for tumor cells. *Chem Pharm Bull (Tokyo)* 59(1):63–71.
13. Gabizon A, et al. (1994) Prolonged circulation time and enhanced accumulation in malignant exudates of doxorubicin encapsulated in polyethylene-glycol coated liposomes. *Cancer Res* 54(4):987–992.
14. Gao ZG, Lee DH, Kim DI, Bae YH (2005) Doxorubicin loaded pH-sensitive micelle targeting acidic extracellular pH of human ovarian A2780 tumor in mice. *J Drug Target* 13(7):391–397.
15. Licciardi M, Cavallaro G, Di Stefano M, Fiorica C, Giammona G (2011) Polyaspartamide-graft-polymethacrylate nanoparticles for doxorubicin delivery. *Macromol Biosci* 11(3):445–454.
16. O'Brien ME, et al.; CAELYX Breast Cancer Study Group (2004) Reduced cardiotoxicity and comparable efficacy in a phase III trial of pegylated liposomal doxorubicin HCl (CAELYX/Doxil) versus conventional doxorubicin for first-line treatment of metastatic breast cancer. *Ann Oncol* 15(3):440–449.
17. Immordino ML, Dosio F, Cattel L (2006) Stealth liposomes: Review of the basic science, rationale, and clinical applications, existing and potential. *Int J Nanomedicine* 1(3):297–315.
18. Ogawara K-I, Un K, Tanaka K-I, Higaki K, Kimura T (2009) In vivo anti-tumor effect of PEG liposomal doxorubicin (DOX) in DOX-resistant tumor-bearing mice: Involvement of cytotoxic effect on vascular endothelial cells. *J Control Release* 133(1):4–10.
19. Lorusso D, et al. (2007) Pegylated liposomal doxorubicin-related palmar-plantar erythrodysesthesia ('hand-foot' syndrome). *Ann Oncol* 18(7):1159–1164.
20. von Moos R, et al. (2008) Pegylated liposomal doxorubicin-associated hand-foot syndrome: Recommendations of an international panel of experts. *Eur J Cancer* 44(6):781–790.
21. Hamad I, Hunter AC, Szebeni J, Moghimi SM (2008) Poly(ethylene glycol)s generate complement activation products in human serum through increased alternative pathway turnover and a MASP-2-dependent process. *Mol Immunol* 46(2):225–232.
22. Szebeni J, et al. (2006) Complement activation-related cardiac anaphylaxis in pigs: role of C5a anaphylatoxin and adenosine in liposome-induced abnormalities in ECG and heart function. *Am J Physiol Heart Circ Physiol* 290(3):H1050–H1058.
23. Ishida T, et al. (2006) Injection of PEGylated liposomes in rats elicits PEG-specific IgM, which is responsible for rapid elimination of a second dose of PEGylated liposomes. *J Control Release* 112(1):15–25.
24. Dams ET, et al. (2000) Accelerated blood clearance and altered biodistribution of repeated injections of sterically stabilized liposomes. *J Pharmacol Exp Ther* 292(3):1071–1079.
25. Dos Santos N, et al. (2004) pH gradient loading of anthracyclines into cholesterol-free liposomes: Enhancing drug loading rates through use of ethanol. *Biochim Biophys Acta* 1661(1):47–60.
26. Gardikis K, Tsimplouli C, Dimas K, Micha-Screttas M, Demetzos C (2010) New chimeric advanced Drug Delivery nano Systems (chi-aDDnSs) as doxorubicin carriers. *Int J Pharm* 402(1–2):231–237.
27. Yadav AK, et al. (2008) Preparation and characterization of HA-PEG-PCL intelligent core-corona nanoparticles for delivery of doxorubicin. *J Drug Target* 16(6):464–478.
28. Patri AK, Kukowska-Latallo JF, Baker JR, Jr. (2005) Targeted drug delivery with dendrimers: Comparison of the release kinetics of covalently conjugated drug and noncovalent drug inclusion complex. *Adv Drug Deliv Rev* 57(15):2203–2214.

29. Boucher C, Gobeil S, Samejima K, Earnshaw WC, Poirier GG (2001) Identification and analysis of caspase substrates: Proteolytic cleavage of poly(ADP-ribose)polymerase and DNA fragmentation factor 45. *Methods Cell Biol* 66:289–306.
30. Koh E, Nakamura T, Takahashi H (2004) Troponin-T and brain natriuretic peptide as predictors for adriamycin-induced cardiomyopathy in rats. *Circ J* 68(2):163–167.
31. Singal PK, Iliskovic N (1998) Doxorubicin-induced cardiomyopathy. *N Engl J Med* 339(13):900–905.
32. Myers CE, et al. (1977) Adriamycin: the role of lipid peroxidation in cardiac toxicity and tumor response. *Science* 197(4299):165–167.
33. Abraham SA, et al. (2005) The liposomal formulation of doxorubicin. *Methods Enzymol* 391:71–97.
34. Chen Y, Bathula SR, Li J, Huang L (2010) Multifunctional nanoparticles delivering small interfering RNA and doxorubicin overcome drug resistance in cancer. *J Biol Chem* 285(29):22639–22650.
35. Gardikis K, et al. (2010) New drug delivery nanosystem combining liposomal and dendrimeric technology (liposomal locked-in dendrimers) for cancer therapy. *J Pharm Sci* 99(8):3561–3571.
36. Ishihara T, et al. (2009) Accelerated blood clearance phenomenon upon repeated injection of PEG-modified PLA-nanoparticles. *Pharm Res* 26(10):2270–2279.
37. Szepeshazi K, et al. (2001) Targeting of cytotoxic somatostatin analog AN-238 to somatostatin receptor subtypes 5 and/or 3 in experimental pancreatic cancers. *Clin Cancer Res* 7(9):2854–2861.
38. Geng Y, et al. (2007) Shape effects of filaments versus spherical particles in flow and drug delivery. *Nat Nanotechnol* 2(4):249–255.
39. Christian DA, et al. (2009) Flexible filaments for in vivo imaging and delivery: Persistent circulation of filomicelles opens the dosage window for sustained tumor shrinkage. *Mol Pharm* 6(5):1343–1352.
40. Wiedemeyer R, Westermann F, Wittke I, Nowock J, Schwab M (2003) Ataxin-2 promotes apoptosis of human neuroblastoma cells. *Oncogene* 22(3):401–411.